International Journal of Thin Film Science and Technology

Volume 10
Issue 3 *Sep. 2021*

Article 14

2021

Molarity Dependent on CVD Misted ZnS Buffer Layer Performance

Fadoua Mansouri
Laboratory of Materials Physics and Subatomic, Faculty of Science, University Ibn Tofail, BP.133-14000 Kénitra, Morocco, fadoua.mansouri@uit.ac.ma

Yassine Khaaissa
Laboratory of Materials Physics and Subatomic, Faculty of Science, University Ibn Tofail, BP.133-14000 Kénitra, Morocco, yassine.khaaissa@uit.ac.ma

Abdelali Talbi
Laboratory of Materials Physics and Subatomic, Faculty of Science, University Ibn Tofail, BP.133-14000 Kénitra, Morocco, abdelali.talbi@gmail.com

Khalid Nouneh
Laboratory of Materials Physics and Subatomic, Faculty of Science, University Ibn Tofail, BP.133-14000 Kénitra, Morocco, khalid.nouneh@uit.ac.ma

Outman El Khouja
Laboratory of Materials Physics and Subatomic, Faculty of Science, University Ibn Tofail, BP.133-14000 Kénitra, Morocco\\ Laboratory of Multifunctional Materials and Structures, National Institute of Materials Physics, Atomistilor 405A, 077125 Magurele, Romania, fadoua.mansouri@uit.ac.ma

Molarity Dependent on CVD Misted ZnS Buffer Layer Performance

Authors

Fadoua Mansouri, Yassine Khaaissa, Abdelali Talbi, Khalid Nouneh, Outman El Khouja, Hassan Ahmoum, Aurelian Catalin Galca, Guojian Li, Qiang Wang, Omar Bajjou, and Mustapha Mabrouki

International Journal of Thin Films Science and Technology

http://dx.doi.org/10.18576/ijtfst/100314

Molarity Dependent on CVD Misted ZnS Buffer Layer Performance

Fadoua Mansouri [1], *Yassine Khaaissa* [1], *Abdelali Talbi* [1,*], *Khalid Nouneh* [1], *Outman El Khouja* [1,2], *Hassan Ahmoum* [3,4], *Aurelian Catalin Galca* [2], *Guojian Li* [3], *Qiang wang* [3], *Omar Bajjou* [5] *and Mustapha Mabrouki* [5]

[1]Laboratory of Materials Physics and Subatomic, Faculty of Science, University Ibn Tofail, BP.133-14000 Kénitra, Morocco
[2] Laboratory of Multifunctional Materials and Structures, National Institute of Materials Physics, Atomistilor 405A, 077125 Magurele, Romania
[3] Key Laboratory of Electromagnetic Processing of Materials (Ministry of Education), Northeastern University, Shenyang, 110819, China
[4]Physics of Materials and Systems Modeling Laboratory (PMSML), Unit Associated at CNRST-URAC: 08, Faculty of Sciences, Moulay Ismail University, B.P, 11201, Zitoune, Meknes, Morocco
[5]Physics department, Faculty of Sciences and Technics, Sultan Moulay Slimane University, Beni Mellal, Morocco

Received: 21 May 2021, Revised: 2 Aug. 2021, Accepted: 4 Aug. 2021.
Published online: 1 Sep. 2021.

Abstract: This paper manifests the synthesis and characterization of zinc sulfur (ZnS) thin films combined with numerical simulation (SCAPS-1D). The synthesis has been done by mixing and depositing Zn and S precursors on a preheated glass substrate (450 °C) with different molar concentrations. X-ray diffraction (XRD) shows the formation of polycrystalline ZnS with a mixed hexagonal/cubic structure. Raman spectroscopy analysis validates the film's purity with a predominant peak at 348 cm^{-1} corresponding to the cubic structure. Composition elements and atomic ratio have been confirmed by the energy dispersive X-ray analysis (EDX). Scanning electronic microscopy (SEM) and atomic force microscopy (AFM) images show uniform and well-arranged spherical grains on the sample's surface with a non-neglected roughness variation. The optical results show high transparency in the visual field of light (≃80%) and a sharp absorption edge in the UV domain. The optical band gap has been considerably decreased with increasing the concentrations reflecting its high dependency on the molarity rate. Numerical modeling results using SCAPS-1D software show that samples corresponding to 0.06 and 0.08 molarity present better performance with an efficiency of 8.94% and 8.9%, respectively.

Keywords: ZnS; Mist CVD; Thin films; Concentration effect; Solar cells; Buffer layer.

1 Introduction

In the last two decades, thin films solar cells have been the main topic of basic and applied research. In a photovoltaic device, there are four layers. In addition to the substrate, which is usually glass, we find the back contact, which is in most cases molybdenum (Mo), the second layer is the absorbent layer with p-type conduction, the third is the buffer layer, and the top one is the transparent conductive oxide (TCO) layer. The buffer layer, which is located between the absorbent and TCO layers, greatly influences the performance of thin-film solar cells [1]. Without it, the efficiency of the directly made junction between the absorbent and the TCO layers will be limited due to the large band offset of the TCO/absorbent layer and the leakage currents caused by the presence of disordered areas at boundaries [2-6].

For this reason, a buffer layer is necessary to reduce the energy barrier between the absorber layer and the TCO. In commercial PV, Cadmium sulfide (CdS) has played this role well for a good time [7]. However, Cadmium is toxic and causes serious environmental problems. Using a toxic material to fabricate an environmentally friendly device has no sense. Hence, it is necessary to search for a non-toxic buffer material suitable for environmental and industrial production. Among materials, ZnS is a promising transition metal with a direct wide band gap (3.5–3.8 eV) [8]; it has a cubic (sphalerite) or hexagonal phase (wurtzite). As a buffer layer, ZnS can reduce ZnS/TCO band offset, and also, it can let all the visible light interact with the absorber layer, which is not the case of CdS.

From an electrical and optical point of view, ZnS is considered among the most interesting materials. It has been

*Corresponding author E-mail: abdelali.talbi@uit.ac.ma

used in electroluminescent devices [9,10], biosensors [11], lasers [12], ultraviolet light-emitting diodes [9], and as a phosphor host [13]. In the field of optics, ZnS can be used in dielectric filters, reflectors, anti-reflection, and coatings due to its high refractive index (2.35) and high transmittance in the visible domain [14-17].

In this stimulating context, several physical and chemical techniques have been used to synthesis ZnS such as electron beam evaporation [18], molecular beam epitaxy [19], Metal-Organic Chemical Vapor Deposition [20,21], SILAR [22], spray pyrolysis [14,23,24], electrodeposition [25], chemical bath deposition [11,26,27] and Mist chemical vapor deposition [28–31].

Ben Nasr et al. [32] have deposited ZnS thin films using the chemical bath deposition (CBD) technique. They have studied the pH effect on structural and optical properties. Their samples have shown a high transmission (~ 70%), and a direct band gap energy around 3.67 eV is obtained for films prepared at pH=11.5. Djelloul et al. [33] have studied the substrate temperature influence on structural, morphological, and optical properties of ZnS thin films prepared by spray pyrolysis technique. They have found that ZnS films have a polycrystalline cubic structure and that the grain size increases with increasing substrate temperature from 350 °C to 500 °C. Mkawi et al. [34] have used the electrodeposition technique to elaborate ZnS films. They have studied the sulfurization temperatures effect on morphological, electrical, and optical properties. They have found that the samples exhibit a zinc blende structure and that the film crystallization has been improved with increasing annealing temperature. Kazuyuki et al. [31] have studied the growth dynamics of zinc sulfide films deposited by the mist chemical vapor deposition (mist-CVD) method with a quartz fine-channel susceptor. They have shown that the type of mist generators and that of susceptors play an essential role in the films' uniformity.

After elaborating the TCO layer (ZnO:Al) using the Mist CVD technique [35], we report now an experimental and numerical study of ZnS thin films as a buffer layer using the same effective method. The effect of precursor's concentration on the structural, optical, and morphological properties have been investigated using X-ray diffraction (XRD) data, Raman, scanning electron microscopy (SEM), energy dispersive spectroscopy (EDS), atomic force microscopy (AFM), and UV-vis measurements. The influence of concentration on ZnS films' conversion efficiency as a buffer layer on solar cells has been evaluated using the SCAPS-1D free simulation package [36]. Other cell layers have been chosen to be ZnO-Al, CZTS, and Mo as TCO, absorbent and back contact, respectively. Section 2 describes the experimental details. Section 3 presents the experimental results. Section 4 shows the numerical modeling findings. Conclusions are given in section 5.

2 Experimental Section

2.1 Growth procedure

ZnS thin films have been deposited on a glass substrate by the Mist CVD technique using zinc chloride and Thiourea as zinc and sulfur sources. Both precursors are dissolved in distilled water under constant agitation, then some drops of HCL are added. The solution has been prepared for the following concentrations: 0.04 M, 0.06 M, 0.08 M, and 0.1 M. The used parameters are regrouped in Table. 1:

Table 1. ZnS thin films' deposition parameters.

Parameters	Value
Deposition temperature (°C)	450°C
Deposition time	30 min
Carrier gas flow rate	2 L/min (N_2)
Dilution gas flow rate	1 L/min (N_2)
Precursors' concentration	0.04 M, 0.06 M, 0.08 M and 0.1 M

Since the quality of the films depends on the substrate surface cleanliness, we have performed a multi-step cleaning operation:

* First wash for 10 min in an ultrasonic acetone bath.
* Second wash for 10 min in an ultrasonic methanol bath.
* Rinsing with distilled water for 5 min.
* Drying the substrates using an oven at 125 °C.

After cleaning the substrates, we put them on the reactor placed on a heater fixed at 450 °C. The prepared solution is misted using two ultrasonic generators. The generated mist pushed to the canal using the carrier gas (N_2) and transported to the reactor using the dilution gas (N_2). After 30 min, we put down the system, and we obtain ZnS thin films. All operation is carried out under a hoover to get rid of exhaust gas. The entire system is detailed in our previous paper [35].

3 Results and Discussion

3.1 Structural Evaluation

The crystal structure of ZnS samples has been analyzed by X-ray diffraction. Figure 1 shows a series of X-ray diffractograms of ZnS samples for concentrations ranging from 0.04 M to 0.1 M. The patterns indicate that all ZnS films are polycrystalline with a predominance of the hexagonal phase along (002) plan for concentrations less than or equal to 0.06 M. For 0.08 M, the phase turns to be cubic ZB along (111) plan. More increasing the molarity to attaint 0.1 M, XRD diagram keeps the ZB phase. Still, another small one corresponding to wurtzite structure along (100) plan appears, indicating the presence of a mixture of hexagonal and cubic phases with a predominance of the cubic one. Generally, ZnS crystallizes in cubic and/or hexagonal form. The phase selectivity (cubic/hexagonal) is influenced by the deposition technique, the processing parameters, and the type of substrate [23,37]. Cubic ZnS

films have been reported by certain authors [1,26,38-42] and hexagonal by others [25,43,44]. ZnS films produced by the Mist CVD technique [28,45] present a mixture of cubic and hexagonal forms. More recently, Anil M. Palve [46] has found a hexagonal phase for thin ZnS layers produced using the Mist CVD technique.

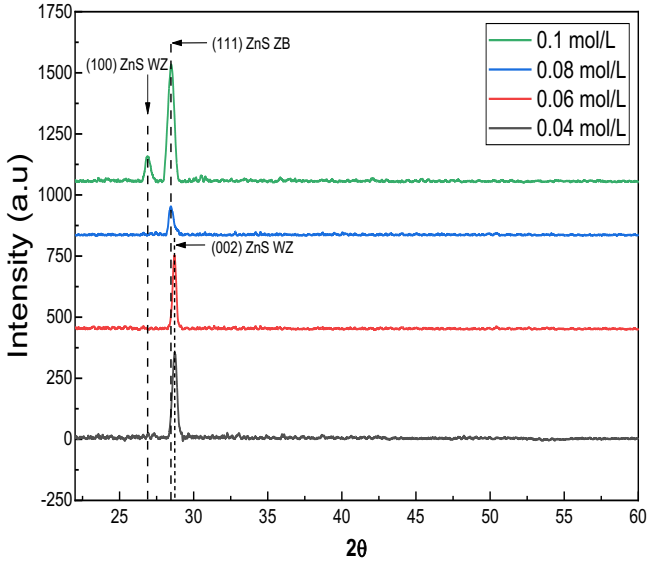

Figure 1. X-ray diffraction spectra of ZnS samples for different concentrations.

For obtaining more structural information, we have calculated the crystallites size "D", the dislocation Density "δ", and the micro-strain "ε" through the following formulas [47,48]:

$$D = \frac{0.94\lambda}{\beta \cos \theta} \quad (1)$$

$$\delta = \frac{1}{D^2} \quad (2)$$

$$\varepsilon = \frac{\beta \cos \theta}{4} \quad (3)$$

Table 2. Crystallite size, dislocation density, and micro strain parameters

Concentration	Crystallite size (nm)	Dislocation Density x 10^{15}(lines/m^2)	Micro-strain x 10^{-3}
0.04	19.29	2.68	3.02
0.06	25.85	1.49	2.24
0.08	17.06	3.43	3.45
0.1	14.64	4.66	4.01

Table.2 shows the data of D, δ, and ε for several concentrations. We note that Crystallite size increases with increasing the solution molarity up to 0.06 M and then decreases. Contrary, it has been observed that the dislocation density and the micro-strain softly decrease until reaching 0.06 M and then increases for 0.08 and 0.1 M. This behavior can be directly correlated with the reduction in material dislocations under 0.06 M. Beyond this value, more defects appear which contracts or expands the nearer lattices by producing local strain close to the defects [49]. A similar behavior, caused by the temperature, has also been found by Offor et al. [50].

A Raman spectroscopic analysis has been done to confirm the structural result and have additional information about the samples' chemical species.

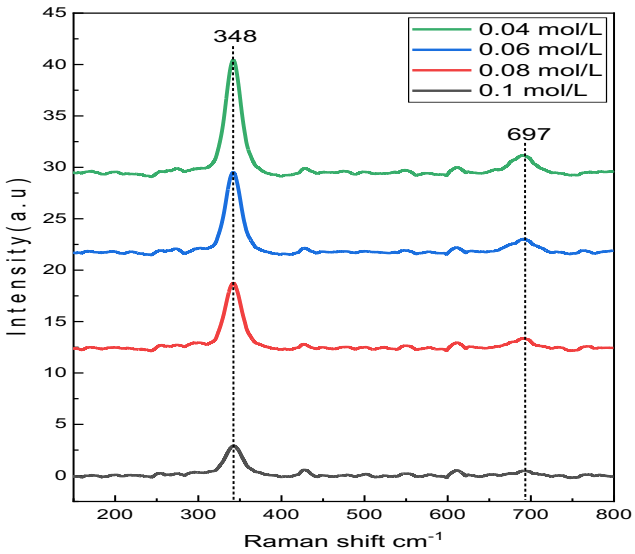

Figure 2. Raman spectra of ZnS thin films with 325 nm excitation

Raman spectroscopy is an advanced technique for investigating the structure of the synthesized material and detecting the secondary phases that cannot be found easily in XRD. The Raman scattering response of ZnS films under UV excitation (λexc= 325 nm) is shown in Fig.2.The main and the intense peak located at 348 cm^{-1} is identified as (LO) vibrational mode of ZnS compound [51,52]. This peak intensity increases as the concentration decreases. Another peak of a second mode is observed at 697 cm^{-1}. This peak vanishes for high concentrations. This has to do with the particles' size; grains with very small sizes show low wavenumber vibrational modes observed by Raman spectroscopy [53]. Besides, No secondary phase peaks (as ZnO) have been observed. The XRD and Raman findings prove that the Mist CVD technique has been successfully synthesized zinc sulfide thin films.

3.2 Optical Properties of ZnS

ZnS use as a buffer layer is governed mainly by its optical properties as the transmission and the optical band gap. Figure 3 contains the optical transmittance of ZnS films at different concentrations in the wavelength range of 300 nm to 1800 nm. We can notice that the sample corresponds to 0.1 M has the lowest transmittance compared to the rest. This transmittance reduction at higher molarity may be attributed to the increase in surface morphology roughness leading to photons scattering increase [54]. And also maybe because at 0.1 M there are two phases wurtzite and Cubic. For samples

deposited with 0.04 M, 0.06 M, and 0.08 M concentrations, we can observe that the transmittance increases as the molarity increases and reaching its maximum value of 88% in the visual field of light (710 nm). This enhancement in the transmittance can be explained by the crystallinity improvement at a corresponding concentration or by reducing the optical scattering caused by the film densification. Besides, in the Infrared domain, all samples show a good transmission. Also, all ZnS films exhibit absorption edges around 310-320 nm.

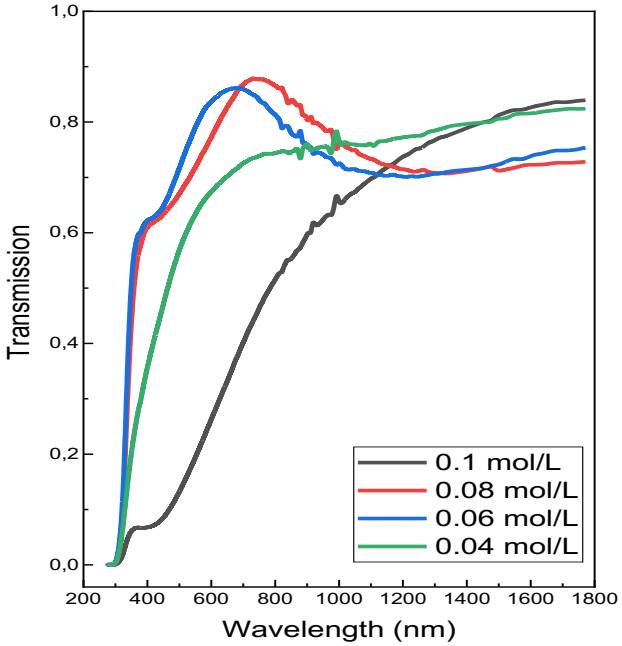

Figure 3. Transmittance spectra of ZnS thin films

To determine the optical band gap, the relation of Tauc [55] between the absorption coefficient α and the energy of incident photon ($h\nu$) has been used. The extrapolation of the plot's first linear part to x-axis is giving the Eg value.

$$\alpha h\nu = A(h\nu - E_g)^n \quad (4)$$

Where A is a constant, n takes ½ or 2 depending on the transition nature. Fig.4 illustrates the extrapolation of the linear part of $(\alpha h\nu)^2$ versus $(h\nu)$ for different concentrations. The obtained Eg values are 3.67 eV, 3.82 eV, 3.8 eV, and 3.5 eV for 0.04 M, 0.06 M, 0.08 M, and 0.1 M respectively.

No linear correlation has been found between the band gap and the increases of the precursors' molarity because of the competition between wurtzite and the cubic structure. Eg goes from 3.67 eV to 3.82 eV when increasing the concentration from 0.04 M to 0.06 M, passing to 0.08 M, Eg slightly decreased to 3.8 eV. Reaching 0.1 M, the band gap drops to the value of 3.5 eV. The remarkable band gap reduction when passing to 0.1 M may have a link to the structural defects in the film giving rise to new allowed states near the conduction band [56]. The founded values are consistent with those reported by Ben Nasr (3.67-3.88 eV) using chemical bath deposition [32], Hwang (3.45-3.79 eV) using RF magnetron sputtering [15], Djelloul (3.89-3.96 eV) using spray pyrolysis [33], and Hennayaka (3.75-3.88 eV) using pulsed electrodeposition [57].

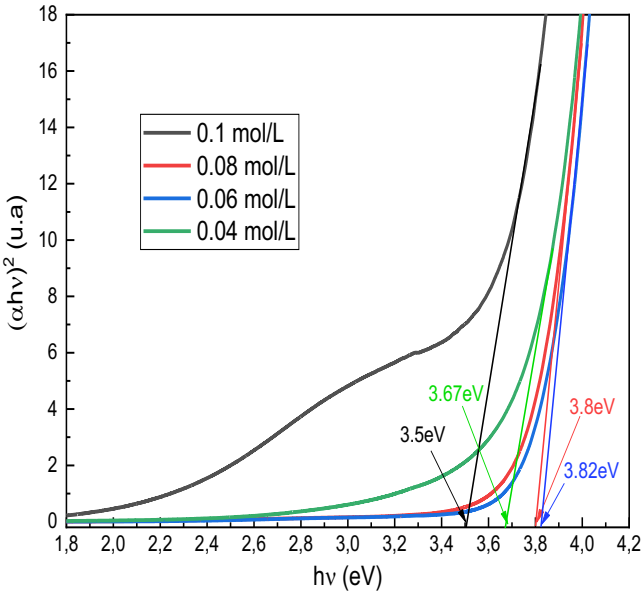

Figure 4. The optical band gap for different concentrations of ZnS thin films

3.3 Morphology Evaluation of ZnS thin solid films

Fig. 5 presents ZnS thin films' morphology for various concentration rates. It is readily apparent that all films have good adhesion to the substrate, high density, and compact particles covering the entire substrate surface without any voids, cavities, or aggregations. We can see that the nanocrystallite has a hexagonal structure for the small concentrations (0.04 and 0.06 M). Increasing the molarity to more than 0.06 M, SEM images reveal the presence of both hexagonal and cubic forms, with a predominance of the cubic shape for 0.1 M concentration. This analysis is consistent with XRD measurement results.

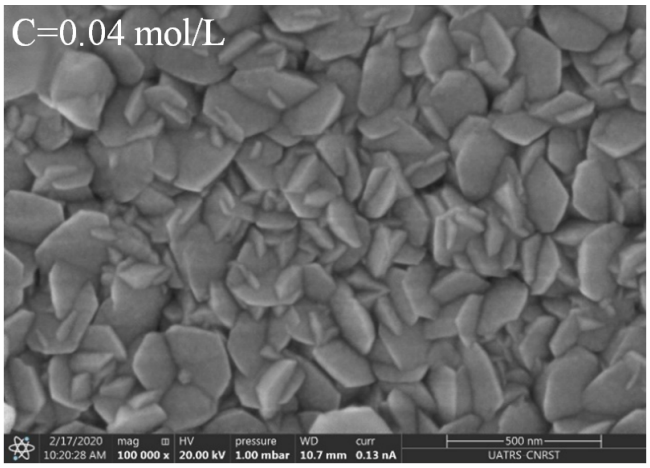

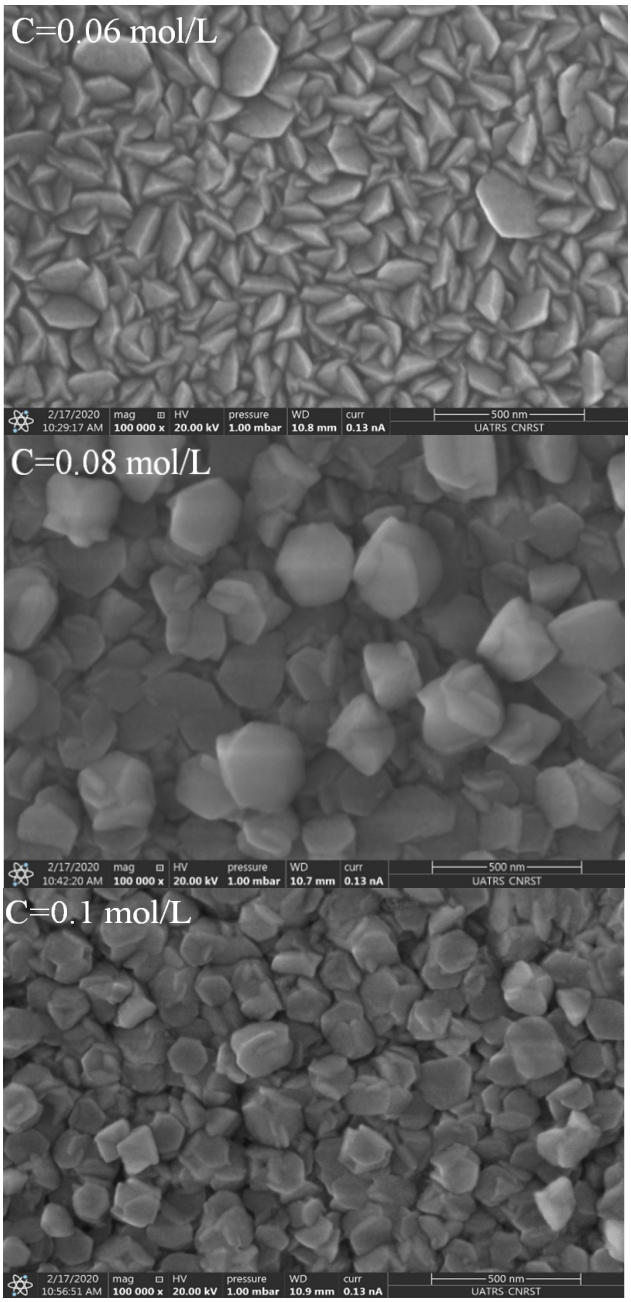

Figure 5. SEM images of ZnS thin films.

To have a clear view of the atomic ratio between S and Zn elements in the deposited films, we have regrouped in Table 3 the percentages and the atomic ratio for different samples. The presented data have been obtained from the EDX analysis. We can remark that all the samples are lightly Zn rich from the given data since their percentage is relatively higher than S, revealing a slight sulfur deficiency. This can be explained by the high volatility of the S element, especially at high temperatures. Another point to outlines is that the S/Zn ratio is almost the same (around 0.6) whatever the molarity rate value. These findings indicate that even the quotient S/Zn is lower than desired, the ZnS compound is obtained without the need for the sulfurization step.

Table 3. Composition information of ZnS thin films

Concentration	0.04 M	0.06 M	0.08 M	0.1 M
Zn (at.%)	61.2	60.2	61.3	64.1
S (at.%)	38.8	39.8	38.7	35.9
S/Zn	0.63	0.66	0.63	0.56

To analyze our samples from another morphological point of view, we have illustrated in Fig.6 the AFM images with their average roughness for different concentration rates. The results confirm the SEM observation about the homogeneity of the surfaces and the uniformity of the crystallites as well as their excellent distribution on the surface. The 3D presentation shows the grains' orthogonality on the surface, indicating the growth perpendicularity relative to the substrate. Besides, it is evident that increasing the precursors' morality modifies the surface conditions and affect the samples' roughness strongly. This later takes the values of 67.84 nm, 21.92 nm, 48.14 nm, and 52.13 nm for 0.04 M, 0.06 M, 0.08 M, and 0.1 M respectively. They have been found to be rough for 0.04 M, become softer for 0.06 M, and turn rough again for 0.08 M and 0.1 M with the appearance of some agglomerations. The black curves on AFM images, which represent the roughness variation for different concentrations, confirm these findings. Indeed, during the nucleation process, surface defects could appear in many ways leading to an unexpected roughness increase [58]. Smooth surface structures have, in general, a remarkable ability to avoid the phenomenon of scattering of incident light which considerably reduces the propagation loss [59].

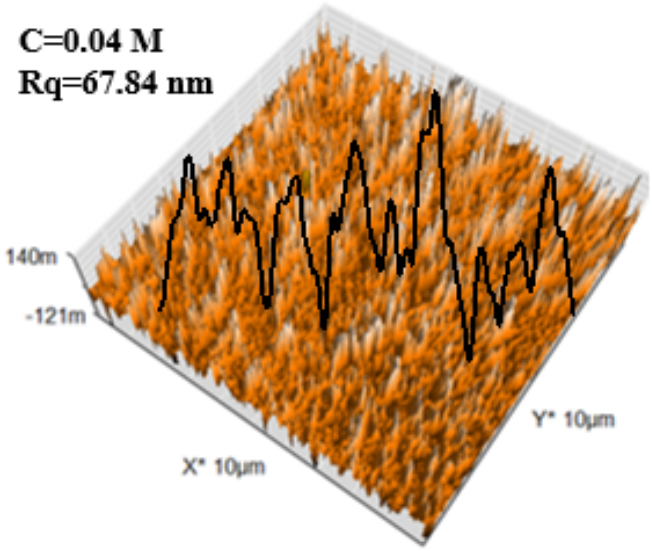

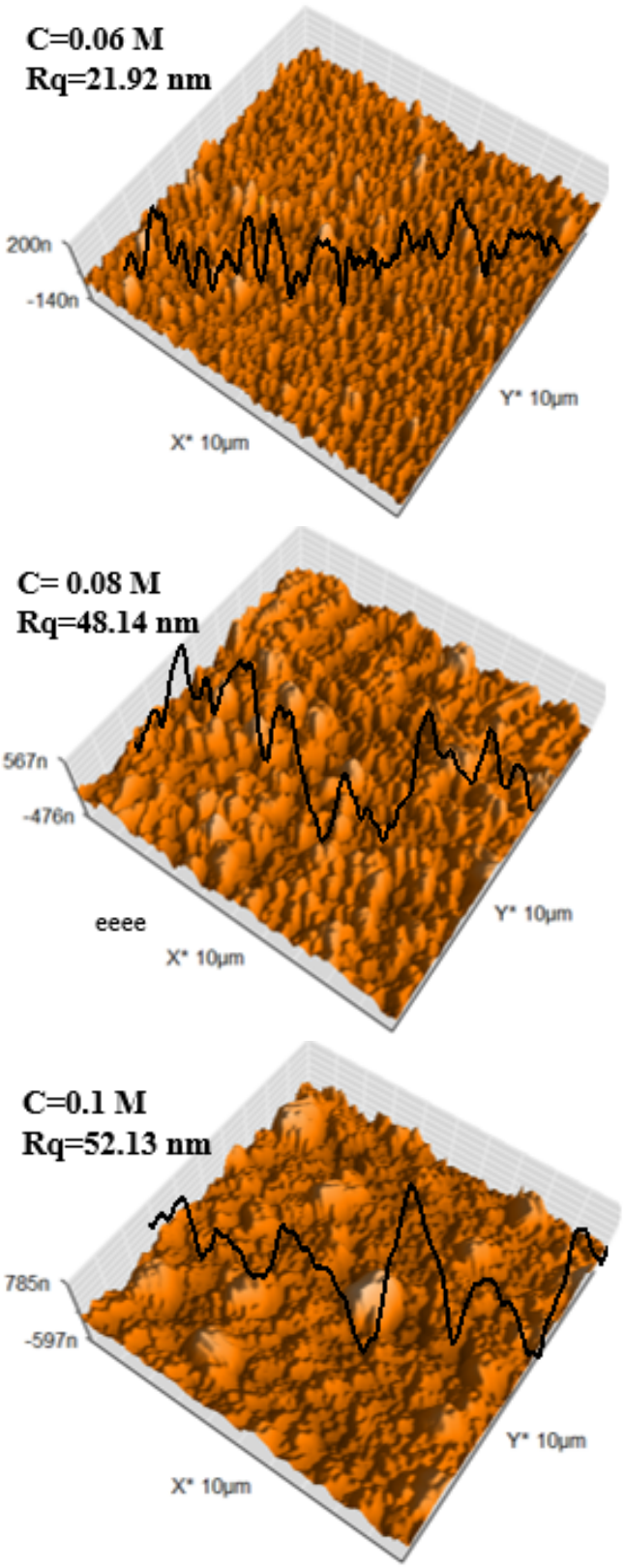

Figure 6. 3D AFM images of ZnS thin films deposited at different concentrations

4 Numerical Simulation

To evaluate our films' performance as buffer layers in solar cells, we have performed a numerical simulation using SCAPS software, which is a program specially developed to simulate the characteristics of the solar cell by giving the variations of Jsc, Voc, FF, and the efficiency parameters.

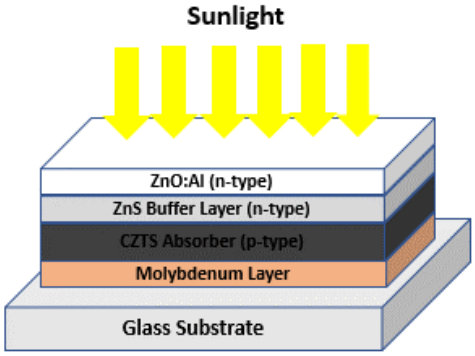

Figure 7. Simplified representation of studied solar cell device

The used materials parameters in this simulation have been taken from the literature and experiment [35,60–62]. The radiation spectrum, the operating temperature, the series resistance (Rs), and the shunt resistance (Rsh) have been chosen respectively as 1.5 G, 300 K, 4.25 Ω.cm^2 and, 400 Ω.cm^2 [60]. Table 4 and 5 show the necessary material and device parameters used in the simulation. Figure 7 shows a simplified representation of the studied solar cell device.

Table 4. Basic material parameters used in the simulation

Parameters	ZnO :Al	ZnS	CZTS
Thickness (µm)	0,483	0,480-0,500	3
Band gap (eV)	3,22	3,5-3,82	1,5
Electron affinity (eV)	4,6	4,13	4,5
Relative dielectric permittivity	9	10	10
CB effective density of states (cm^{-3})	$2,2\times10^{18}$	$2,2\times10^{18}$	$2,2\times10^{18}$
VB effective density of states (cm^{-3})	$1,8\times10^{19}$	$1,8\times10^{19}$	$1,8\times10^{19}$
Electron thermal velocity (cm/s)	1×10^{7}	1×10^{7}	1×10^{7}
Hole thermal velocity (cm/s)	1×10^{7}	1×10^{7}	1×10^{7}
Electron mobility (cm²/Vs)	100	100	60
Hole mobility (cm²/Vs)	25	25	20
Donor density ND (cm^{-3})	1.2×10^{20}	1×10^{17}	10
Acceptor density NA (cm^{-3})	1×10^{5}	0	7×10^{16}
Absorption coefficient	Exp. Data	Exp. Data	$4,25\times10^{4}$

Table 5. Basic device parameters used in the simulation

Contacts	Front metal contact	Back metal contact
Work function	Flat band	Mo 5eV
Surface Recombination Velocity of electron	10^7 cm/s	10^7 cm/s
Surface Recombination Velocity of hole	10^7 cm/s	10^7 cm/s

Forming a hetero-junction means that the Fermi level of all films aligns and thus, all the bands line up with respect to the vacuum level. The energy band's discontinuity is the main matter for the hetero-junction based thin film solar cells devices, as the carrier's collection at the metal contacts is concerned. Under lighting, free carriers are created, and the Fermi level splits to quasi level [63]. This separation is the origin of the open-circuit voltage (Voc) of the device, and the short circuit current (Jsc) is related to the solar spectral irradiance [60]. The flat band has been used as the front contact. During the simulation, SCAPS software automatically computes the work function value of the used flat band. Regarding the back contact, a work function of 5 eV has been considered for Molybdenum (Mo). Mo has been chosen due to its high conductivity and optical reflectivity to bounce photons back to the absorber layer [64]. Before starting our analysis, we may recall that this part aims is analyzing the buffer layer concentration effect on the solar cells' performance. The molarity's impact in this later is reflected in the band gap, thickness, and absorbance coefficient. All other parameters are taken from our other works or literature.

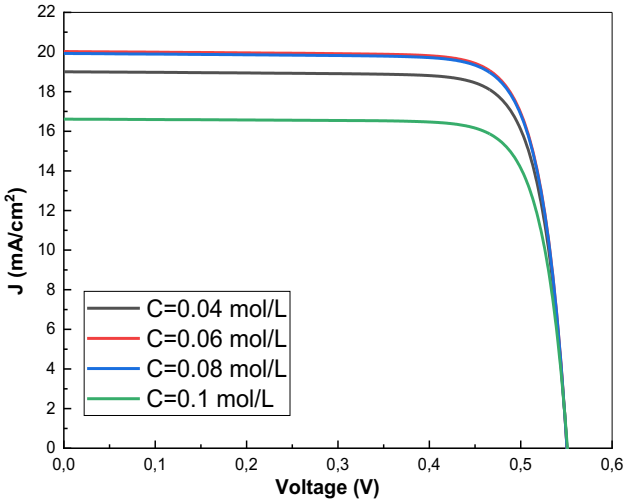

Figure 8. J-V characteristics of ZnO:Al/ZnS/CZTS/Mo solar cells for different ZnS concentrations

Figure 8 shows J-V characteristics of ZnO:AL/ZnS/CZTS/Mo solar cell for different ZnS layers. We may note that Jsc decreases as the buffer layer concentration increases. This may have a link with ZnS films' thickness which can enhance their absorbance and caused a significant photon loss. Indeed, a thick buffer layer decreases the number of photons transmitted to the absorbent layer; thus, few electron-hole pairs will be generated [65]. Besides, we can see that the samples corresponding to 0.06 and 0.08 M have the best and almost the same J-V characteristics.

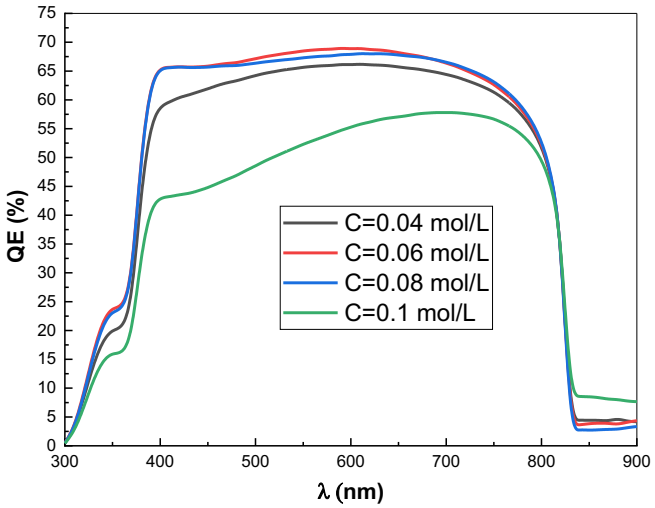

Figure 9. The quantum efficiency for several concentrations of ZnS buffer layer.

The solar cell efficiency is quantified by internal (IQE) and external quantum efficiency (EQE). The IQE is the ratio between the collected electrons and the number of absorbed photons. IQE helps to predict the total current generated under the solar spectrum. On the other side, the EQE reflects the solar cell optical performance as well as the charge generation with respect to the incident light [66]. Fig. 9 shows the external quantum efficiency given as QE (Or IPCE) by SCAPS software. Seeing the curves, we can remark that the QE, in the wavelength range of 300 nm to 850 nm, increases when the concentrations increase from 0.04 M to 0.06 M and 0.08 M. Increase more the molarity from 0.08 to 0.1 M decrease considerably the QE. Indeed, the buffer layer plays a vital role in cell efficiency since it controls the photons number reaching the absorbent layer, and the QE is very sensitive to this parameter [65].

Table 6. Solar cell performance parameters for different buffer layer concentrations.

Sample	Voc (V)	J_{SC} (mA/cm^2)	FF (%)	η (%)	η_R (%)
0.04 M	0.552	19.00	80.89	8.495	6.756
0.06 M	0.552	20.02	80.86	8.945	7.071
0.08 M	0.552	19.92	80.86	8.902	7.041
0.1 M	0.553	16.61	81.07	7.449	5.998

Table 6. shows the solar cell performance parameters as a function of buffer layer molarity. The solar cell's efficiency increases slightly when the concentration increases from 0.04 M to 0.06 M, stabilizes around the value of 8.9% for 0.06 M and 0.08 M molarity and then undergoes a sharp

decrease down to the value of 7.44%. The decrease in efficiency can be explained by the reduction of Jsc since Voc and FF quantities remain almost constant. The efficiency reached for the concentrations of 0.06 and 0.08 M can be considered good and can be improved by varying other deposition parameters. Using the same buffer and absorbent layers (ZnS and CZTS) Cherouana et al. [67] have found an efficiency of 8.02%. Series and parallel resistances significantly influence solar cell performance, particularly on the fill factor (FF) and Jsc. The series resistance (Rs) originates from the bulk resistance, the front and back contacts resistance, and extra circuit resistances from connections and terminals. The parallel resistance knowing as shunt resistance (Rsh) is coming from the leakage currents. Impurities and the junction's non-idealities lead to a partial junction shorting, especially near the cell borders [68]. To see the influence of series and parallel resistance on the cell performance, we have calculated the cell efficiency taking into account those resistances. Based on table 6 values, we note that when the series and shunt resistance takes non-zero values which equal by default 4.25 $\Omega.cm^2$ and 400 $\Omega.cm^2$ respectively, the efficiency decreases significantly. This is due to the fact that the Rsh and the Rs affect the J–V characteristics leading to a reduction in the output value. Thereby, to obtain the higher efficiency of solar cells, it is recommended to take low Rs and high Rsh.

4 Conclusions

This work has been carried out to contribute in improving the ZnS buffer layer for solar cell devices. In this context, ZnS thin films have been synthesized on a glass substrate heated to 450 °C for different concentrations using the Mist CVD technique and then numerically simulated using SCAPS-1D package. The structural characterization revealed that 0.08 molarity is the optimal concentration, with a cubic "zinc blende" structure along the plane (111) as the preferred growth orientation. The Raman spectrum has proved the ZnS structure and shown that no secondary phase has been detected. The optical properties of ZnS films have revealed a very interesting transmission in the visible domain with an extrapolated gap value of 3.8 eV for the sample deposited at 0.08 M. The SEM and AFM images have shown that the resulting films are homogeneous, uniform, relatively rough, and well adherent to the substrate. The simulation results have demonstrated that the thickness, band gap, and absorption coefficient of the buffer layer have an important effect on cell performance. The maximum efficiency, which has been found equal to 8.9%, is obtained by the two samples synthesized with a molarity of 0.06 and 0.08. The numerical results are consistent with the experimental ones and confirm that ZnS films produced with 0.08 M deserve to be proposed as an effective and promising buffer layer for solar cell devices.

Acknowledgement

The research was supported by the Moroccan Ministry of Higher Education and Research and CNRST in the PPR/37/2015 project framework.

References

[1] S. D. Sartale, B. R. Sankapal, M. Lux-Steiner, and A. Ennaoui, 'Preparation of nanocrystalline ZnS by a new chemical bath deposition route,' Thin Solid Films, **480**, 168–172, 2005.

[2] A. D. Katnani and G. Margaritondo, "Microscopic study of semiconductor heterojunctions: Photoemission measurement of the valance-band discontinuity and of the potential barriers," Phys. Rev. B, **28**, 1944–1956, 1983.

[3] F. Fenske, K. Kliefoth, L. Elstner, and B. Selle, "ZnO/c-Si heterojunction interface tuning by interlayers," in Materials Research Society Symposium - Proceedings, **426**, 135–140, 1996.

[4] K. Ramanathan et al., "Junction formation in CuInSe[sub 2]-based thin-film devices," AIP Conference Proceedings, **462**, 9–16, 2009.

[5] T. Nakada, "Nano-structural investigations on Cd-doping into Cu(In,Ga)Se2 thin films by chemical bath deposition process," Thin Solid Films, **361**, 346–352, 2000.

[6] L. Weinhardt et al., "Band alignment at the CdS Cu (In,Ga) S2 interface in thin-film solar cells," Appl. Phys. Lett., **86**, 1–3, 2005.

[7] P. K. Vidyadharan Pillai and K. P. Vijayakumar, "Characterization of CuInSe2/CdS thin-film solar cells prepared using CBD," Sol. Energy Mater. Sol. Cells, **51**, 47–54, 1998.

[8] F. Abdi and H. Savaloni, "Investigation of the growth conditions on the nano-structure and electrical properties of ZnS chiral sculptured thin films," Appl. Surf. Sci., **330**, 74–84, 2015.

[9] Y. Luo, G. Duan, M. Ye, Y. Zhang, and G. Li, "Poly(ethylene glycol)-mediated synthesis of hollow ZnS microspheres," J. Phys. Chem. C, **112**, 2349–2352, 2008.

[10] K. Manzoor, S. R. Vadera, N. Kumar, and T. R. N. Kutty, "Multicolor electroluminescent devices using doped ZnS nanocrystals," Appl. Phys. Lett., **84**, 284–286, 2004.

[11] R. Sahraei and S. Darafarin, "Preparation of nanocrystalline Ni doped ZnS thin films by ammonia-free chemical bath deposition method and optical properties," J. Lumin., **149**, 170–175, 2014.

[12] S. Biswas, T. Ghoshal, S. Kar, S. Chakrabarti, and S. Chaudhuri, "ZnS nanowire arrays: Synthesis, optical and field emission properties," Cryst. Growth Des., **8**, 2171–2176, 2008.

[13] L. P. Wang and G. Y. Hong, "New preparation of zinc sulfide nanoparticles by solid-state method at low temperature," Mater. Res. Bull., **35**, 695–701, 2000.

[14] S. Liu, H. Zhang, and M. T. Swihart, "Spray pyrolysis synthesis of ZnS nanoparticles from a single-source precursor," Nanotechnology, **20**, 235603, 2009.

[15] D. H. Hwang, J. H. Ahn, K. N. Hui, K. S. Hui, and Y. G. Son, "Structural and optical properties of ZnS thin films deposited by RF magnetron sputtering," Nanoscale Res. Lett., **7**, 26, 2012.

[16] A. M. Kute and S. A. Waghuley, "Photovoltaic application of ZnS loaded silicon dioxide rich composites," Mater. Des., **116**, 1–7, 2017.

[17] A. T. Salih, A. A. Najim, M. A. H. Muhi, and K. R. Gbashi, "Single-material multilayer ZnS as anti-reflective coating for solar cell applications," Opt. Commun., **388**, 84–89, 2017.

[18] B. Abdallah, K. Alnama, and F. Nasrallah, "Deposition of ZnS thin films by electron beam evaporation technique, effect of thickness on the crystallographic and optical properties," Mod. Phys. Lett. B, **33**, 1950034, 2019.

[19] S. Schön, M. Chaichimansour, W. Park, T. Yang, B. K. Wagner, and C. J. Summers, "Homogeneous and δ-doped ZnS:Mn grown by MBE," J. Cryst. Growth, **175**, 598–602, 1997.

[20] J. Fang et al., "MOCVD growth of non-epitaxial and epitaxial ZnS thin films," Appl. Surf. Sci., **70**, 701–706, 1993.

[21] W. S. Kook, H. Y. Seok, S. L. Seung, and I. W. Shim, "Preparation of ZnS thin film using Zn(dithiocarbamate)2 precursors by MOCVD method," Bull. Korean Chem. Soc., **26**, 1582–1584, 2005.

[22] A. Ates, M. A. Yildirim, M. Kundakci, and A. Astam, "Annealing and light effect on optical and electrical properties of ZnS thin films grown with the SILAR method," Mater. Sci. Semicond. Process., **10**, 281–286, 2007.

[23] B. Elidrissi, M. Addou, M. Regragui, A. Bougrine, A. Kachouane, and J. C. Bernède, "Structure, composition and optical properties of ZnS thin films prepared by spray pyrolysis," Mater. Chem. Phys., **68**, 175–179, 2001.

[24] H. H. Afifi, S. A. Mahmoud, and A. Ashour, "Structural study of ZnS thin films prepared by spray pyrolysis," Thin Solid Films, **263**, 248–251, 1995.

[25] R. Torres-Ricárdez et al., "Electrodeposited stoichiometric zinc sulfide films," Ceram. Int., **46**, 10490–10494, 2020.

[26] G. Arandhara, J. Bora, and P. K. Saikia, "Effect of pH on the crystallite size, elastic properties and morphology of nanostructured ZnS thin films prepared by chemical bath deposition technique," Mater. Chem. Phys., **241**, 122277, 2020.

[27] J. Cheng, D. B. F. Fan, H. Wang, B. W. Liu, Y. C. Zhang, and H. Yan, "Chemical bath deposition of crystalline ZnS thin films," Semicond. Sci. Technol., **18**, 676–679, 2003.

[28] K. Uno, Y. Yamasaki, and I. Tanaka, "Growth mechanisms of zinc oxide and zinc sulfide films by mist chemical vapor deposition," Appl. Phys. Express, **10**, 015502, 2017.

[29] K. Okita, K. Inaba, Z. Yatabe, and Y. Nakamura, "Structural characteristics of a non-polar ZnS layer on a ZnO buffer layer formed on a sapphire substrate by mist chemical vapor deposition," Jpn. J. Appl. Phys., **57**, 065503, 2018.

[30] K. Uno, Y. Asano, and I. Tanaka, "Photoluminescence thermal quenching properties of zinc sulfide grown by mist chemical vapor deposition," Phys. status solidi, **254**, 1600544, 2017.

[31] K. Uno, Y. Yamasaki, P. Gu, and I. Tanaka, "Growth of zinc sulfide by mist chemical vapor deposition depending on mist size and thermal conditions in susceptor," Phys. status solidi, **13**, 448–451, 2016.

[32] T. Ben Nasr, N. Kamoun, M. Kanzari, and R. Bennaceur, "Effect of pH on the properties of ZnS thin films grown by chemical bath deposition," Thin Solid Films, **500**, 4–8, 2006.

[33] A. Djelloul et al., "Properties study of ZnS thin films prepared by spray pyrolysis method," J. Nano- Electron. Phys., **7**, 4, 2015.

[34] E. M. Mkawi, K. Ibrahim, M. K. M. Ali, M. A. Farrukh, and A. S. Mohamed, "Electrodeposited ZnS Precursor Layer with Improved Electrooptical Properties for Efficient Cu2ZnSnS4 Thin-Film Solar Cells," J. Electron. Mater., **44**, 3380–3387, 2015.

[35] Y. Khaaissa, K. Fathi, A. Talbi, K. Nouneh, K. El Mabrouk, and A. Taleb, "Ultrasonic Spray-Assisted CVD Growth of Highly Transparent and Conductive Aluminum-Doped ZnO," Surf. Rev. Lett., **27**, 12, 2020.

[36] M. Burgelman, P. Nollet, and S. Degrave, "Modelling polycrystalline semiconductor solar cells," Thin Solid Films, **361**, 527–532, 2000.

[37] R. D. Pike et al., "Preparation of zinc sulfide thin films by ultrasonic spray pyrolsis from bis(diethyldithiocarbamato) zinc(II)," Thin Solid Films, **224**, 221–226, 1993.

[38] A. Ashour, H. H. Afifi, and S. A. Mahmoud, "Effect of some spray pyrolysis parameters on electrical and optical properties of ZnS films," Thin Solid Films, **248**, 253–256, 1994.

[39] M. Tonouchi, Y. Sun, T. Miyasato, H. Sakama, and M. Ohmura, "Room-temperature synthesis of zns: Mn films by 82 plasma chemical sputtering," Jpn. J. Appl. Phys., **29**, 2453–2456, 1990.

[40] J. A. Lahtinen, A. Lu, T. Tuomi, and M. Tammenmaa, "Effect of growth temperature on the electronic energy band and crystal structure of ZnS thin films grown using atomic layer epitaxy," J. Appl. Phys., **58**, 1851–1853, 1985.

[41] J. Lee, S. Lee, S. Cho, S. Kim, I. Y. Park, and Y. D. Choi, "Role of growth parameters on structural and optical properties of ZnS nanocluster thin films grown by solution growth technique," Mater. Chem. Phys., **77**, 254–260, 2003.

[42] A. I. Trejo-Ramos, I. J. González-Chan, and A. I. Oliva, "Physical properties of chemically deposited ZnS thin films: Role of the solubility curves and species distribution diagrams," Mater. Sci. Semicond. Process., **118**, 105207, 2020.

[43] L. Schönbrodt and K. Reichelt, "Preparation of ZnS films by reactive sputtering and their investigation by electron microscopy and Rutherford backscattering," Thin Solid Films, **81**, 45–52, 1981.

[44] Y. Bouznit, Y. Beggah, A. Boukerika, A. Lahreche, and F. Ynineb, "New co-spray way to synthesize high quality ZnS films," Appl. Surf. Sci., **284**, 936–941, 2013.

[45] M. A. Ehsan et al., "Surface morphological and photoelectrochemical studies of ZnS thin films developed from single source precursors by aerosol assisted chemical

vapour deposition," Thin Solid Films, **540**, 1–9, 2013.

[46] A. M. Palve, "Deposition of Zinc Sulfide Thin Films From Zinc(II) Thiosemicarbazones as Single Molecular Precursors Using Aerosol Assisted Chemical Vapor Deposition Technique," Front. Mater., **6**, 46, 2019.

[47] M. Zayed, A. M. Ahmed, and M. Shaban, "Synthesis and characterization of nanoporous ZnO and Pt/ZnO thin films for dye degradation and water splitting applications," Int. J. Hydrogen Energy, **44**, 17630–17648, 2019.

[48] S. Lalitha, R. Sathyamoorthy, S. Senthilarasu, A. Subbarayan, and K. Natarajan, "Characterization of CdTe thin film - Dependence of structural and optical properties on temperature and thickness," in Solar Energy Materials and Solar Cells, **82**, 187–199, 2004.

[49] S. B. Kulkarni, U. M. Patil, R. R. Salunkhe, S. S. Joshi, and C. D. Lokhande, "Temperature impact on morphological evolution of ZnO and its consequent effect on physico-chemical properties," J. Alloys Compd., **509**, 3486–3492, 2011.

[50] P. O. Offor, B. A. Okorie, F. I. Ezema, V. S. Aigbodion, C. C. Daniel-Mkpume, and A. D. Omah, "Synthesis and characterization of nanocrystalline zinc sulphide thin films by chemical spray pyrolysis," J. Alloys Compd., **650**, 381–385, 2016.

[51] W. G. Nilsen, "Raman spectrum of cubic ZnS," Phys. Rev., **182**, 838–850, 1969.

[52] A. Fairbrother et al., "ZnS grain size effects on near-resonant Raman scattering: Optical non-destructive grain size estimation," CrystEngComm, **16**, 4120–4125, 2014.

[53] T. Hurma, "Effect of boron doping concentration on structural optical electrical properties of nanostructured ZnO films," J. Mol. Struct., **1189**, 1–7, 2019.

[54] S. R. Chalana, V. Ganesan, and V. P. Mahadevan Pillai, "Surface plasmon resonance in nanostructured Ag incorporated ZnS films," AIP Adv., **5**, 107207, 2015.

[55] J. Tauc, R. Grigorovici, and A. Vancu, "Optical Properties and Electronic Structure of Amorphous Germanium," Phys. status solidi, **15**, 627–637, 1966.

[56] M. Y. Nadeem and W. Ahmed, "Optical Properties of ZnS Thin Films," Turkish Journal of Physics, **24**, 651-659, 2000.

[57] H. M. M. N. Hennayaka and H. S. Lee, "Structural and optical properties of ZnS thin film grown by pulsed electrodeposition," Thin Solid Films, **548**, 86–90, 2013.

[58] P. Roy, J. R. Ota, and S. K. Srivastava, "Crystalline ZnS thin films by chemical bath deposition method and its characterization," Thin Solid Films, **515**, 1912–1917, 2006.

[59] Z. B. Fang, Z. J. Yan, Y. S. Tan, X. Q. Liu, and Y. Y. Wang, "Influence of post-annealing treatment on the structure properties of ZnO films," Appl. Surf. Sci., **241**, 303–308, 2005.

[60] A. D. Adewoyin, M. A. Olopade, O. O. Oyebola, and M. A. Chendo, "Development of CZTGS/CZTS tandem thin film solar cell using SCAPS-1D," Optik (Stuttg)., **176**, 132–142, 2019.

[61] B. Abd El Halim, A. Mahfoud, and D. Mohammed Elamine, "Numerical analysis of potential buffer layer for Cu2ZnSnS4 (CZTS) solar cells," Optik (Stuttg)., **204**, 164155, 2020.

[62] M. B. Hosen, A. N. Bahar, M. K. Ali, and M. Asaduzzaman, "Modeling and performance analysis dataset of a CIGS solar cell with ZnS buffer layer," Data Br., **14**, 246–250, 2017.

[63] M. Patel and A. Ray, "Enhancement of output performance of Cu 2ZnSnS 4 thin film solar cells - A numerical simulation approach and comparison to experiments," Phys. B Condens. Matter, **407**, 4391–4397, 2012.

[64] O. K. Simya, A. Mahaboobbatcha, and K. Balachander, "A comparative study on the performance of Kesterite based thin film solar cells using SCAPS simulation program," Superlattices Microstruct., **82**, 248–261, 2015.

[65] P. Chelvanathan, M. I. Hossain, and N. Amin, "Performance analysis of copper-indium-gallium-diselenide (CIGS) solar cells with various buffer layers by SCAPS," in Current Applied Physics, **10**, S387–S391, 2010.

[66] K. Chakraborty, M. G. Choudhury, and S. Paul, "Numerical study of Cs2TiX6 (X = Br−, I−, F− and Cl−) based perovskite solar cell using SCAPS-1D device simulation," Sol. Energy, **194**, 886–892, 2019.

[67] A. Cherouana and R. Labbani, "Study of CZTS and CZTSSe solar cells for buffer layers selection," Appl. Surf. Sci., **424**, 251–255, 2017.

[68] H. Heriche, Z. Rouabah, and N. Bouarissa, "New ultra thin CIGS structure solar cells using SCAPS simulation program," Int. J. Hydrogen Energy, **42**, 9524–9532, 2017.